A new demodulation technique for optical fiber interferometric sensors with [3 × 3] directional couplers

Tingting Liu (刘亭亭), Jie Cui (崔 杰), Desheng Chen (陈德胜), Ling Xiao (肖 灵), and Dexing Sun (孙德兴)

Institute of Acoustics, Chinese Academy of Sciences, Beijing 100080

Received March 15, 2007

Optical fiber interferometric sensors based on [3 × 3] couplers have been used in many fields. A new technique is proposed to demodulate output signals of this kind of sensors. The technique recovers the signal of interest by fitting coefficients of elliptic (Lissajous) curves between each fiber pair. Different from other approaches, this technique eliminates the dependence on the idealization of [3 × 3] coupler, provides enhanced tolerance to the variance of photoelectric converters, and is anti-polarization in a certain extent. The main algorithm has been successfully demonstrated both by numerical simulation and experimental result.

OCIS codes: 060.2370, 070.6020, 060.1810, 120.3180.

Single-mode fiber interferometric sensors have drawn a great deal of attention due to their high accuracy, high sensitivity, and immunity of electromagnetic disturbance. Optical fiber interferometric sensors based on [3 × 3] couplers have been used to detect acoustic, magnetic, temperature perturbations and delamination in composites[1,2]. Use of [3 × 3] directional couplers in interferometer has been proposed early in 1980[3], and it was reported that it could solve the signal fading problem[3−5]. Sheem *et al.* analyzed the waveguide theory of [3 × 3] couplers, and gave the output expressions in which the coefficients of three channels are equal[4]. Furthermore, scattering matrix theory was also used to describe the property of [3×3] couplers[6,7]. This theory is simple and straightforward compared with the waveguide theory, but the latter is clearer and exacter in physical conception.

The key of interferometic fiber-optic sensors is demodulation technique. In 1982, Koo *et al.* proposed a simple demodulator[8] according to the output expressions of [3 × 3] coupler given by Sheem. References [9 − 11] described a conventional demodulation technique which involved differentiation, cross-multiplication, summing and integration etc. and required different gains for three outputs, when the output phase differences were 120°. Although the demodulation methods described above seem straightforward, there are many difficulties in implementation. For example, imperfection during the fabrication of [3 × 3] couplers will lead the splitting ratio to deviate from 1:1:1 and the output differences to deviate from ±120°. The asymmetry of couplers and the variance of photoelectric converters will both cause amplitude fluctuations at the outputs. These factors will degrade the demodulation performance and measurement precision.

In this paper, a new demodulation technique is presented. We establish the output mathematical model of [3×3] fiber coupler which is a little different from Sheem's result using waveguide theory, and further obtain general expressions synthesizing the practical condition of coupler. The demodulation algorithm is described, which utilizes the elliptic curve between any two of the three outputs.

Figure 1 is an optical fiber hydrophone using Mach-Zehnder interferometer (MZI) with C_1 a [2 × 2] coupler and C_2 a [3 × 3] directional coupler. Let $z = 0$ denote the input port of [3 × 3] coupler and $z = L$ denote its output port. Let $a_i(z)$ $(i = 1, 2, 3)$ be the complex amplitudes of three waves in the [3×3] coupler at the reference point z. $a_i(z)$ are governed by a set of linear differential equations[3,4]

$$\frac{\mathrm{d}a_i}{\mathrm{d}z} + jK_{i,i+1}a_{i+1} + jK_{i,i+2}a_{i+2} = 0,$$
$$i = 1, 2, 3, \quad i + 3 := i, \tag{1}$$

where $K_{i,k}(= K_{k,i})$ is the coupling coefficient between the ith and the kth waveguides, and := means equivalence. Assuming that $K_{12} = K_{23} = K_{31} = K$ for mathematical simplicity, then the solutions for a_i in this case are[3]

$$a_i(z) = c_i \mathrm{e}^{jKz} + b\mathrm{e}^{-2jKz}, \quad \sum_{i=1}^{3} c_i = 0, \tag{2}$$

where c_i and b are constants.

According to the principle of MZI, we assume that the inputs of [3 × 3] directional coupler are $a_1(0) = r_1\mathrm{e}^{j\phi_1}$, $a_2(0) = r_2\mathrm{e}^{j(\phi_1+\phi)}$, $a_3(0) = 0$. The first leg $a_1(0)$ corresponds to the reference arm with the initial phase ϕ_1 and amplitude r_1; the second leg $a_2(0)$ corresponds to the signal arm where ϕ denotes the phase shift relative

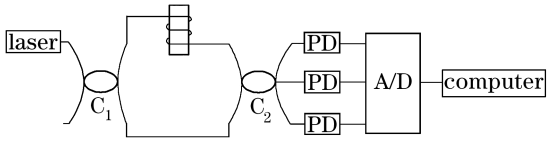

Fig. 1. Schematic diagram of optical fiber hydrophone with MZI. PD: photoelectric detector.

to the reference arm caused by signal of interest such as ambient physical change and r_2 denotes the amplitude; the third leg $a_3(0)$ is free. Furthermore, $r_1 \neq r_2$ represents that C_1 in Fig. 1 is nonideal, with amplitudes of two outputs different.

According to Eq. (2), the output power at $z = L$ can be expressed as

$$P_i = \frac{1}{2}|a_i(L)|^2 = \frac{1}{2}[|c_i|^2 + |b|^2 + 2\Re(c_i b^* \mathrm{e}^{j\beta})], \quad i = 1, 2, 3, \tag{3}$$

where $\Re(\cdot)$ is real-part operator, b^* means complex conjugate of b, and $\beta = 3KL$. c_i $(i = 1, 2, 3)$ and b can be derived by substituting $a_i(0)$ to Eq. (2), and Eq. (3) can be rewritten as

$$\begin{aligned}
P_1 &= \frac{1}{18}[5r_1^2 + 2r_2^2 + 2(2r_1^2 - r_2^2)\cos\beta \\
&\quad + r_1 r_2\sqrt{40 - 8\cos\beta - 32\cos^2\beta}\cos(\pi + \phi - \psi)], \\
P_2 &= \frac{1}{18}[2r_1^2 + 5r_2^2 + 2(-r_1^2 + 2r_2^2)\cos\beta \\
&\quad + r_1 r_2\sqrt{40 - 8\cos\beta - 32\cos^2\beta}\cos(\pi + \phi + \psi)], \\
P_3 &= \frac{1}{18}[2r_1^2 + 2r_2^2 + 2(-r_1^2 - r_2^2)\cos\beta \\
&\quad + (4r_1 r_2 - 4r_1 r_2\cos\beta)\cos\phi],
\end{aligned} \tag{4}$$

where $\tan\psi = \frac{3\sin\beta}{\cos\beta - 1}$, ψ is a constant related to the coupling coefficient and coupler's length L, and the direct current (DC) terms of P_1 and P_2 are not identical, which is different from Ref. [4].

The similar result can be obtained in the case that the three coupling coefficients are not identical, but the derivation will be more complicated[4].

In Eq. (4), the DC coefficients and the coefficients of cosine term are constantly related to K, L, r_1, r_2, but they will change with the rotation of the polarization state of each beam[12] or the fluctuation of light source. Additionally, the three photoelectric conversion circuits could not be ensured totally same, so synthetically, we can simplify the output electric signals as

$$\begin{cases} V_1 = A_1 + B_1'\cos(\pi + \phi - \psi) \\ V_2 = A_2 + B_2'\cos(\pi + \phi + \psi) \\ V_3 = A_3 + B_3'\cos\phi \end{cases}. \tag{5}$$

Define $U_i = B_i'/A_i$ $(0 < U_i < 1)$, which denotes the visibility of interferometric fringe, and changes randomly between 0 and 1 along with the variety of polarization state[12].

Equations (4) and (5) also indicate the output phase differences of $[3 \times 3]$ coupler. Let $\Delta\theta_{i,j}$ $(i, j = 1, 2, 3)$ denote the phase difference between the ith and jth channel signals. When the coupling coefficients are identical, it can be found that $\Delta\theta_{1,2} = \pm 2\psi$, $\Delta\theta_{1,3} = \Delta\theta_{2,3} = \pi \mp \psi$, i.e. the $[3 \times 3]$ coupler is partial symmetrical. Under ideal condition, where $KL = \frac{\pm 2\pi + 6n\pi}{9}$ or $\frac{2n\pi}{3}$, $\psi = \pm\frac{\pi}{3}$, $\Delta\theta_{1,2} = \Delta\theta_{1,3} = \Delta\theta_{2,3} = \frac{2\pi}{3}$, the $[3 \times 3]$ coupler is full symmetrical. But, actual couplers are lossy and rarely perfectly symmetrical, thus phase differences are not entirely identical. Generally, Eq. (5) can be rewritten as

$$\begin{cases} V_1 = A_1 + B_1'\cos(\phi + \Delta\theta_{1,3}) \\ V_2 = A_2 + B_2'\cos(\phi - \Delta\theta_{2,3}) \\ V_3 = A_3 + B_3'\cos\phi \end{cases} \tag{6}$$

or

$$\begin{cases} V_1 = A_1 + B_1\cos\phi - C_1\sin\phi \\ V_2 = A_2 + B_2\cos\phi + C_2\sin\phi \\ V_3 = A_3 + B_3\cos\phi \end{cases}, \tag{7}$$

where

$$B_1/C_1 = \cot(\Delta\theta_{1,3}), \quad B_2/C_2 = \cot(\Delta\theta_{2,3}). \tag{8}$$

In Eq. (7), any two equations form an elliptic function because of trigonometric function. Take V_2 and V_3 as example, the normalized coefficients of the formed elliptic function and the coefficients of standard elliptic function $x^2 + \alpha_1 xy + \alpha_2 y^2 + \alpha_3 x + \alpha_4 y + \alpha_5 = 0$ are compared as Table 1. α_i $(i = 1, 2, 3, 4, 5)$ can be obtained by least square method (LSM) using enough sample data, then A_2, B_2, C_2, A_3, B_3 can be solved through Table 1 by

$$\begin{cases} A_2 = (\alpha_1\alpha_4 - 2\alpha_2\alpha_3)/(4\alpha_2 - \alpha_1^2) \\ A_3 = (\alpha_1\alpha_3 - 2\alpha_4)/(4\alpha_2 - \alpha_1^2) \\ C_2 = \pm\sqrt{A_2^2 + \alpha_1 A_2 A_3 + \alpha_2 A_3^2 - \alpha_5} \\ B_3 = C_2/\sqrt{\alpha_2 - \frac{1}{4}\alpha_1^2} \\ B_2 = -\frac{1}{2}\alpha_1 B_3 \end{cases}. \tag{9}$$

In the same way, we can get A_1, B_1, C_1. Substituting them into Eq. (7), we can get $\sin\phi$ and $\cos\phi$, and further their derivatives. At last, the signal of interest ϕ is recovered by integrating $\phi' = \cos\phi(\sin\phi)' - \sin\phi(\cos\phi)'$. Additionally, with A_i, B_i, C_i $(i = 1, 2, 3)$, the phase difference $\Delta\theta_{1,3}$ and $\Delta\theta_{2,3}$ can be obtained through Eq. (8).

When the algorithm is implemented, A_i, B_i, C_i are solved periodically using the same length of data until all data are processed, so the obtained A_i, B_i, C_i can represent approximatively the amplitude of output signals of $[3 \times 3]$ coupler.

Numerical simulation was carried out to validate the algorithm. Parameters in Eq. (7) are chosen as $A_1 = 11$, $A_2 = 16$, $A_3 = 6.5$, $\Delta\theta_{1,3} = 132°$, and $\Delta\theta_{2,3} = 105°$, to simulate an asymmetrical coupler; $U_i = 0.9\cos(2\pi t) + 0.51$ changes slowly between 0.02 and 1 to simulate the

Table 1. Comparison between Coefficients of Elliptic Function

Item	Normalized Coefficient	Regression Coefficient
x^2	1	1
xy	$-\frac{2B_2}{B_3}$	α_1
y^2	$(\frac{B_2}{B_3})^2 + (\frac{C_2}{B_3})^2$	α_2
x	$-2A_2 + A_2\frac{B_2}{B_3}A_3$	α_3
y	$2A_2\frac{B_2}{B_3} - 2(\frac{B_2}{B_3})^2 A_3 + 2(\frac{C_2}{B_3})^2 A_3$	α_4
Constant	$A_2^2 - 2A_2\frac{B_2}{B_3}A_3 + (\frac{B_2}{B_3})^2 A_3^2$ $+(\frac{C_2}{B_3})^2 A_3^2 - C_2^2$	α_5

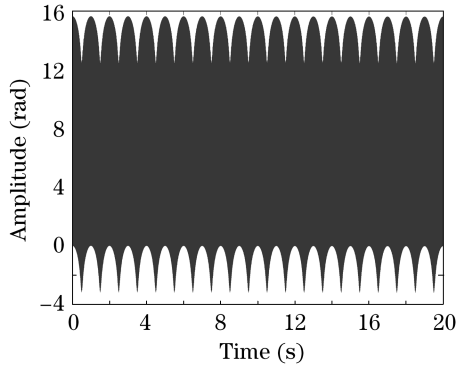

Fig. 2. Demodulation signal in numerical simulation.

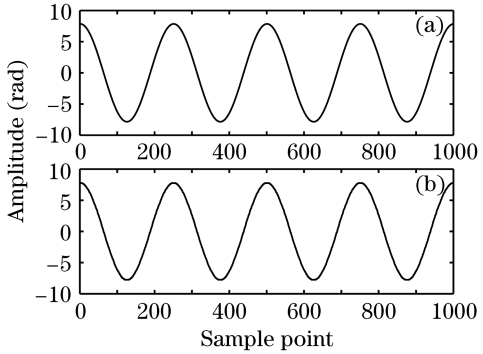

Fig. 3. (a) Original simulated signal and (b) demodulated signal after high-pass filter.

decline of interferometric signal caused by the change of polarization state; the modulation signal is $\phi(t) = 2.5\pi\cos(200\pi t)$.

The demodulated signal is illustrated as Fig. 2, in which the low-frequency envelope is caused by the add-up error of A_i, B_i, C_i $(i = 1, 2, 3)$ obtained through LSM, and has similar frequency component with U_i. The segments of original signal and demodulated one after a high-pass filter are displayed in Fig. 3, and they agree well. If only the interferometric signal does not totally vanish, the demodulation algorithm is very effective.

Affected by environment factor like pressure and temperature etc., U_i may change randomly, i.e. the polarization state is random. Let U_i be a uniform distribution with different ranges, and the mean-square root error δ and correlation coefficient ρ of original and demodulated signal are used to evaluate the performance of proposed algorithm. The results are shown in Table 2, indicating that the demodulation effectiveness is still acceptable if the change of polarization is not very serious.

Through the above two simulations, the proposed algorithm is proved to be anti-polarization in a certain extent.

In laboratory, an optical fiber hydrophone with MZI was used to test the proposed technique. The experiment

Table 2. δ and ρ when U_i Changes in Different Ranges

Range of U_i	$0-1$	$0.3-1$	$0.5-1$	$0.7-1$	$0.90-1$
δ	0.1129	0.0403	0.0189	0.0129	0.0104
ρ	0.8914	0.9608	0.9818	0.9878	0.9901

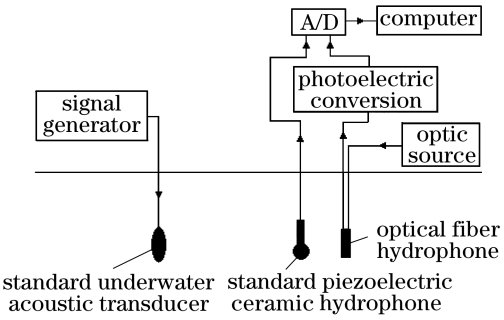

Fig. 4. Experimental setup.

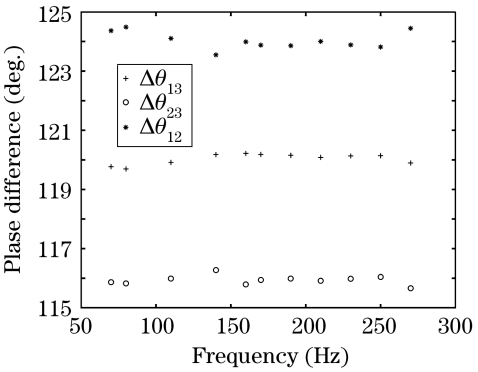

Fig. 5. Phase differences in different modulation frequencies.

was conducted as shown in Fig. 4. Signal generator generates a sinusoidal voltage, which is transmitted to a transducer, then the transducer emits acoustic signal underwater. The acoustic signal is recorded simultaneously by optical fiber hydrophone and piezoelectric ceramic hydrophone that are placed in close position. The output signals of both hydrophones are collected into computer to demodulate. The optic source is a solid laser, with wavelength of 1550 nm, bandwidth of 2 MHz (thus the coherent length is 150 m), and output power of 3 mW. The used optical fiber is single mode and the sensing probe is mandrel type with air cavity[12].

Firstly we processed signals with different modulating frequency, and obtained the phase differences of $[3 \times 3]$ coupler respectively shown in Fig. 5. Obviously, they deviate from 120°, i.e. the $[3 \times 3]$ coupler is asymmetrical. In fact, the coupler is an offgrade product chosen specially for experiment. Considering the error during the experiment, it can be thought that the phase differences are not affected by the modulating frequency.

Then, the demodulation technique was used to process the outputs of optical fiber hydrophone with modulating frequency 170 Hz and sampling rate of 25 kHz. The three channels of outputs of $[3 \times 3]$ coupler are shown in Fig. 6, which shows that the output signals are unstable with A_i changing slowly. Figure 7 shows the magnified singals, and their frequencies are relative with both modulation signal's frequency and amplitude. The bigger the amplitude, the higher the output frequency, so the sampling rate will affect the dynamic range of hydrophone[13]. The three elliptic curves (Lissajous curve) formed by each pair of outputs of $[3 \times 3]$ coupler during 0.1 s are illustrated in Fig. 8. During this time, A_i is almost changeless, and the roughness and width of three curves indicate the random

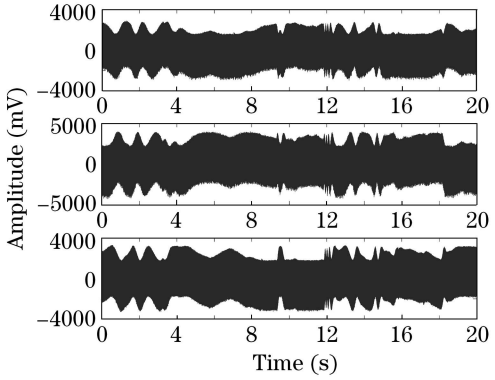

Fig. 6. Three output signals of [3 × 3] coupler.

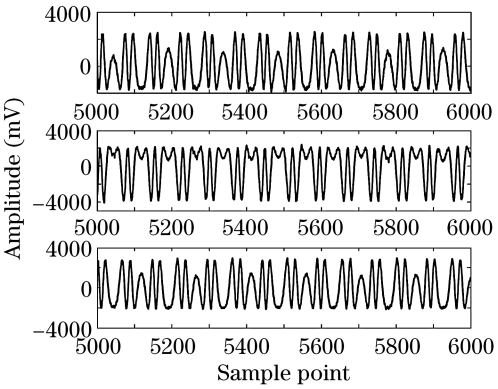

Fig. 7. Three output signals of [3 × 3] coupler after magnification.

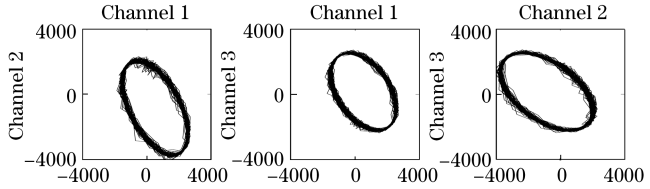

Fig. 8. Elliptic curves (Lissajous curves) between any two channels of the three outputs.

fluctuation of B_i and C_i caused by the change of polarization state. Otherwise, the shape of each curve indicates the output phase difference.

The output of piezoelectric ceramic hydrophone and signals of optical fiber hydrophone demodulated respectively by the new algorithm and the conventional one[10] are illustrated in Fig. 9. It can be found that the new technique is more effective than the conventional one. The proposed algorithm is still valid though the phase differences deviate from 120°, the DC components of [3 × 3] coupler's outputs fluctuate, and the polarization state changes. The similar results can also be obtained for other modulating frequencies from 60 to 1000 Hz.

In this paper, a new demodulation technique utilizing elliptic curve is presented, and the output phase difference of [3 × 3] coupler is also discussed. In contrast to conventional demodulation technique, the new one does not depend on the phase difference of 120° of symmetrical [3 × 3] coupler, does not need to calibrate

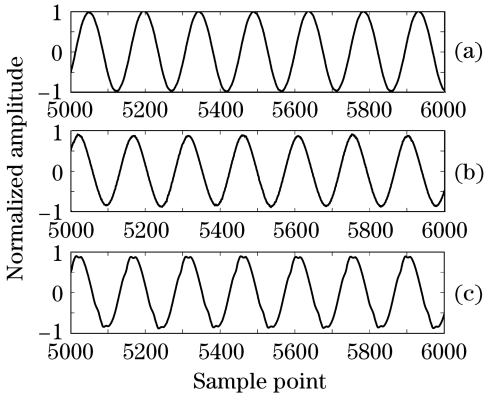

Fig. 9. (a) Output of piezoelectric ceramic hydrophone, (b) signals of optical fiber hydrophone demodulated by the new algorithm and (c) the conventional one.

the parameters of coupler and adjust the gains for coupler's outputs. It is anti-polarization in a certain extent and provides enhanced tolerance to the imperfection of [3×3] coupler and the difference of photoelectric converters. Thus, the cost of research and fabrication can be reduced enormously. The new demodulation technique can be applied to phase interferometer sensor, and expanded to fiber Bragg grating (FBG) sensor using unbalanced MZI. However, the add-up error and the dynamic range of hydrophone still deserve to study further.

This work was supported by the National Natural Science Foundation of China under Grant No. 60673152. T. Liu's e-mail address is ttliu@mail.ioa.ac.cn.

References

1. Y. Jiang and S. Xiao, Journal of Test and Measurement Technology (in Chinese) **18,** 200 (2004).
2. Y. Jiang and T. Jiang, Opt. Technique (in Chinese) **30,** 464 (2004).
3. S. K. Sheem, Appl. Phys. Lett. **37,** 869 (1980).
4. S. K. Sheem, J. Appl. Phys. **52,** 3865 (1981).
5. S. K. Sheem, T. G. Giallorenzi, and K. Koo, Appl. Opt. **21,** 689 (1982).
6. R. G. Priest, IEEE J. Quantum Electron. **18,** 1601 (1982).
7. B. Jiao, Z. Wang, and S. Zheng, Laser & Infrared (in Chinese) **34,** 298 (2004).
8. K. P. Koo, A. B. Tveten, and A. Dandridge, Appl. Phys. Lett. **41,** 616 (1982).
9. R. M. Keolian, S. L. Garrett, and C. B. Cameron, "Demodulators for optical fiber interferometers with [3 × 3] outputs" US Patent 5,313,266 (May 17, 1994).
10. Y. Jiang, Y. Lou, and H. Wang, Acta Photon. Sin. (in Chinese) **27,** 152 (1998).
11. Y. Jiang and S. Chen, Acta Opt. Sin. (in Chinese) **24,** 1487 (2004).
12. M. Ni, "*Investigation of the key technologies of f iber optic hydrophone*" PhD Thesis (Institute of Acoustics, CAS, 2003) PP.35 – 40.
13. J. Cui and L. Xiao, Technical Acoustics **25,** (Suppl.) 511 (2006).